Original Article

Central Asian Journal of Medical Sciences
CAJMS

Cent Asian J Med Sci. 2026 Jun;12(2):12-23 https://doi.org/10.24079/CAJMS.2026.02.002

CT-based radiomics combined with deep learning for preoperative differentiation of clear cell and non–clear cell renal cell carcinoma: Internal and external validation study

Enkhbold Sereejav[1], Purevdorj Otgonbayar[2], Telmen Khuvituguldur[2], Sodgerel Bold[2], Shiirevnyamba Avirmed[1], Gonchigsuren Dagvasumberel[1], Oyunbold Lamid-Ochir[2]

[1]Mongolian National University of Medical Sciences, Ulaanbaatar, Mongolia;
[2]Diagnostic Imaging Center, The First Central Hospital of Mongolia, Ulaanbaatar, Mongolia.

Submitted date: Mar 8, 2025
Accepted date: May 28, 2026

Corresponding Author:
Oyunbold Lamid-Ochir (MD., Ph.D.)
Diagnostic Imaging Center, The First Central Hospital of Mongolia, Ulaanbaatar, Mongolia
E-mail: olamidochir@gmail.com
ORCID: https://orcid.org/0000-0002-0709-3794

Running Title: CT radiomics for RCC subtype differentiation

Objective: Accurate preoperative differentiation of renal cell carcinoma (RCC) subtypes remains challenging with conventional computed tomography (CT) owing to overlapping features. This study evaluated CT-based radiomics combined with deep learning for differentiation of clear cell RCC (ccRCC) from non–clear cell RCC (non-ccRCC), using internal and external validation. **Methods:** This retrospective, single-center study included an internal cohort of 121 patients with histopathologically confirmed RCC (84 ccRCC, 37 non-ccRCC) and an independent external cohort of 73 patients. All underwent preoperative multiphasic contrast-enhanced CT (128-slice Ingenuity). Corticomedullary-phase tumors were segmented in 3D Slicer by two radiologists; inter-observer reliability used the intraclass correlation coefficient (ICC). In total, 122 radiomic features were extracted (first-order, GLCM, GLRLM, GLSZM, GLDM, shape). Least absolute shrinkage and selection operator (LASSO) regression selected features for a deep learning–based classification model. Diagnostic efficacy was assessed by receiver operating characteristic (ROC) curve analysis. **Results:** Inter-observer agreement was excellent (ICC = 0.91; 95% CI, 0.87–0.94). In the internal cohort, the model achieved an area under the curve (AUC) of 0.92, sensitivity 83.3%, specificity 92.3%, and accuracy 86.0%. GLRLM features were most discriminative (AUC = 0.91, $p < .001$), followed by first-order uniformity (AUC = 0.88) and variance (AUC = 0.86). In the external cohort, performance remained robust (AUC = 0.86, sensitivity 82.0%, specificity 80.0%, accuracy 80.8%), confirming generalizability. **Conclusion:** CT-based radiomics combined with deep learning demonstrates high diagnostic performance for differentiating ccRCC from non-ccRCC, generalizing across internal and external datasets. This non-invasive approach may serve as a valuable imaging biomarker supporting clinical decision-making and personalized treatment planning.

Keywords: Renal cell carcinoma; Radiomics; Deep learning; Computed tomography; Clear cell RCC; Subtype differentiation; External validation

Introduction

Renal cell carcinoma (RCC) represents approximately 85–90% of all primary renal

malignancies in adults and accounts for 1–3% of all cancers worldwide.[1,2] Its incidence has steadily increased over recent decades, partly due to the widespread use of cross-sectional imaging modalities. RCC encompasses a heterogeneous group of tumors with distinct histopathological subtypes, most commonly clear cell RCC (ccRCC), papillary RCC, and chromophobe RCC. These subtypes differ significantly in genetic alterations, biological behavior, response to therapy, and clinical outcomes, making accurate characterization essential for optimal patient management.[3,4]

The differentiation of RCC subtypes prior to surgical intervention has important clinical implications. Clear cell RCC is typically associated with a more aggressive clinical course and higher metastatic potential, whereas non–clear cell subtypes often demonstrate more indolent behavior.[3] Preoperative identification of tumor subtype can influence surgical decision-making, including the choice between partial and radical nephrectomy, as well as guide targeted and immunotherapeutic strategies. Furthermore, accurate subtype prediction contributes to risk stratification and personalized treatment planning.[4–8] In addition to subtype classification, preoperative prediction of WHO/ISUP or Fuhrman nuclear grade using CT-based radiomics has also been reported to provide prognostic information and support individualized treatment decisions.[9–12]

Contrast-enhanced CT is the standard imaging modality for detecting and staging renal masses.[1,2] Multiphasic CT protocols provide valuable anatomical and functional information; however, conventional image interpretation is primarily qualitative and limited in capturing intratumoral heterogeneity. Overlapping imaging features among RCC subtypes further complicate accurate differentiation, often necessitating invasive histopathological confirmation.[13,14]

Radiomics has emerged as a promising approach to overcome these limitations by extracting high-dimensional quantitative features from medical images. These features, including first-order statistics and texture-based metrics such as GLCM and GLRLM, allow comprehensive characterization of tumor phenotype beyond visual assessment.[15,16] Radiomics enables non-invasive quantification of tumor heterogeneity, which correlates with histopathological and molecular characteristics. The integration of artificial intelligence (AI), particularly machine learning techniques, has further enhanced the predictive capability of radiomics. Several studies have demonstrated the feasibility of CT-based radiomics for RCC subtype differentiation with high diagnostic accuracy.[17–22] However, most studies are limited by single-center designs and lack of external validation, which restricts their clinical generalizability. [23]

Therefore, the aim of this study was to evaluate the diagnostic performance of CT-based radiomics combined with deep learning for preoperative differentiation of RCC subtypes and to assess its potential as a non-invasive imaging biomarker for clinical decision-making, with both internal and external validation.

Materials and Methods

Study Design and Population

This retrospective single-center study was conducted at the Diagnostic Imaging Center and the Urology–Andrology Center of The First Central Hospital of Mongolia (Ulaanbaatar, Mongolia), a tertiary referral institution, between January 2021 and December 2024. The study protocol was reviewed and approved by the Ethics Committee of the Mongolian National University of Medical Sciences (approval No. 2023/3-04). Because of the retrospective design and use of fully de-identified imaging and clinical data, the requirement for written informed consent was waived by the institutional review board. All procedures were conducted in accordance with the principles of the Declaration of Helsinki. Patient confidentiality was maintained throughout the study: all imaging data were anonymized prior to analysis, and access to identifiable information was restricted to two investigators.

Inclusion and Exclusion Criteria

Inclusion criteria were: (1) adult patients (≥18 years) with renal masses who underwent preoperative multiphasic contrast-enhanced CT at our institution; (2) subsequent surgical resection (partial or radical nephrectomy) with definitive histopathological diagnosis of RCC or related renal neoplasm; (3) CT performed within 30 days prior to surgery; and (4) availability of corticomedullary-phase images of diagnostic quality.

Exclusion criteria were: (1) prior treatment for the index renal mass (e.g., ablation, chemotherapy, or radiotherapy) before CT; (2) suboptimal image quality due to motion or beam-hardening artifacts; (3) tumor diameter <1 cm precluding reliable segmentation; (4) absence of corticomedullary-phase imaging; and (5) incomplete pathological or clinical data. Patient selection and enrollment are summarized in Figure 1.

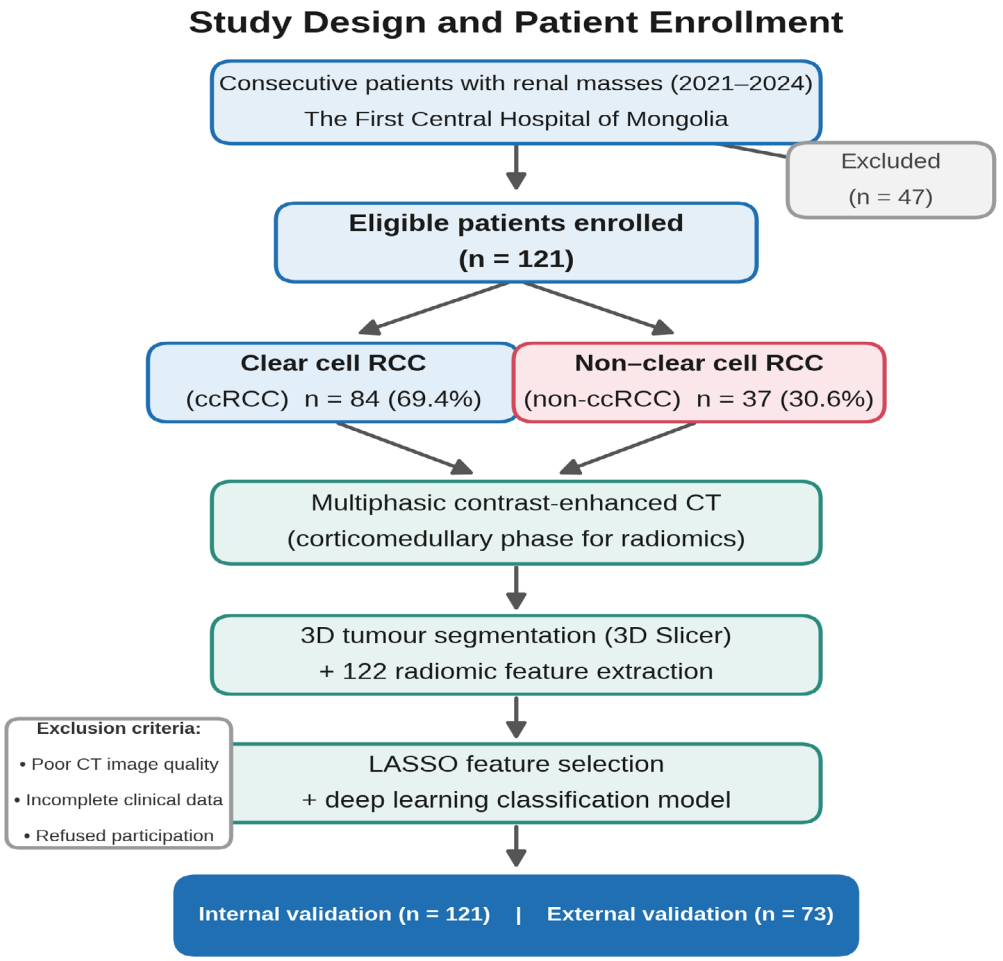

Figure 1. Study design and patient enrollment flowchart. A total of 121 patients with histopathologically confirmed RCC were enrolled and categorized into ccRCC (n=84) and non-ccRCC (n=37) groups. All patients underwent multiphasic contrast-enhanced CT followed by 3D tumor segmentation, radiomic feature extraction, LASSO feature selection, and deep learning-based classification. Internal (n=121) and external (n=73) validation cohorts were used to assess diagnostic performance.

CT Acquisition Protocol

All CT examinations were performed using a 128 Slice CT scanner (Ingenuity; Philips Healthcare, Netherland). A standardized four-phase protocol was used: unenhanced, corticomedullary (25–40 s), nephrographic (70–90 s), and delayed (3–5 min) phases. Acquisition parameters were: tube voltage 120 kVp; tube current modulation 100–500 mA with noise index 12; rotation time 0.5 s; pitch 0.813; collimation 0.5 mm × 80; matrix 512 × 512.

Nonionic iodinated contrast material (iohexol, Omnipaque 300; GE HealthCare, Cork, Ireland; 300 mg I/mL) was administered intravenously at a dose of 1.2 mL/kg body weight using an automated power injector at a flow rate of 3.5 mL/s, followed by a 30 mL saline flush. The corticomedullary phase was selected for radiomic analysis because of its optimal tumor-to-parenchyma contrast.[13,14]

Tumor Segmentation and Inter-observer Reproducibility

Three-dimensional tumor segmentation was performed using the open-source software 3D Slicer (version 5.2.2; Brigham and Women's Hospital, Boston, MA, USA; www.slicer.org). Regions of interest (ROIs) were manually delineated slice-by-slice along the tumor boundary on axial corticomedullary-phase images to generate a volume of interest (VOI). Adjacent normal renal parenchyma, vessels, calcifications, and artifacts were carefully excluded.

To evaluate inter-observer reproducibility, all tumors were

independently segmented by two radiologists with 8 and 12 years of abdominal imaging experience, respectively. These radiologists were blinded to each other's results and the histopathological diagnosis. The inter-observer agreement of the extracted radiomic features was quantified using the intraclass correlation coefficient (ICC, two-way random-effects, absolute agreement). Features with an ICC of 0.75 or higher were retained for subsequent analysis; those with lower agreement were excluded. The overall inter-observer ICC for the retained feature set was 0.91 (95% CI, 0.87–0.94), reflecting excellent reproducibility.

Radiomic Feature Extraction

Radiomic features were extracted from the segmented VOIs using PyRadiomics (version 3.0.1; open-source, https://pyradiomics.readthedocs.io) implemented in Python (version 3.9; Python Software Foundation, Wilmington, DE, USA). Prior to feature extraction, images were resampled to an isotropic voxel size of 1 × 1 × 1 mm using B-spline interpolation, and intensity values were normalized and discretized to a fixed bin width of 25 Hounsfield units to ensure reproducibility. A total of 122 quantitative features were computed, encompassing first-order statistics, GLCM, GLRLM, GLSZM, GLDM, neighborhood gray-tone difference matrix (NGTDM), and shape-based descriptors.[16,17]

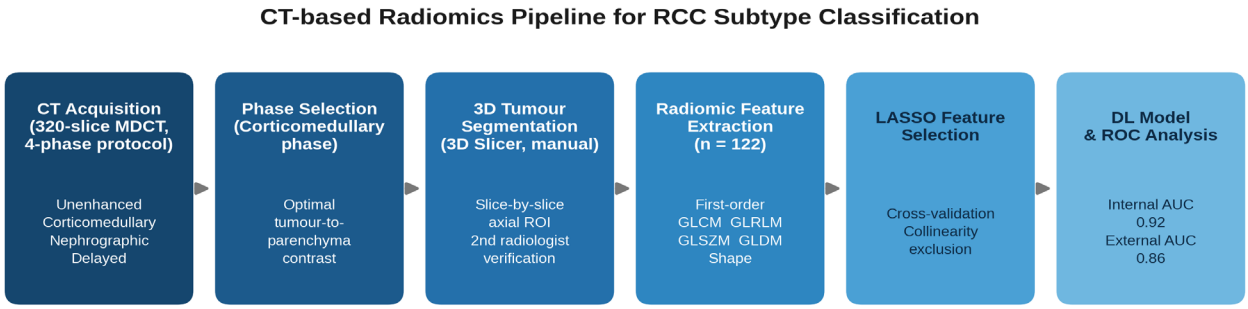

Figure 2. CT-based radiomics pipeline for RCC subtype classification, showing six sequential steps: (1) multiphasic CT acquisition (320-slice MDCT, four-phase protocol); (2) corticomedullary-phase selection; (3) manual 3D tumor segmentation by two radiologists with ICC verification; (4) extraction of 122 quantitative radiomic features (first-order, GLCM, GLRLM, GLSZM, GLDM, NGTDM, shape); (5) LASSO-based feature selection; and (6) deep learning classification with ROC analysis.

Feature Selection and Model Development

To reduce dimensionality and prevent overfitting, feature selection was performed using LASSO regression with 10-fold cross-validation. Highly collinear features (Pearson $|r| > 0.90$) were removed prior to LASSO, and the regularization parameter (λ) was selected to minimize cross-validation deviance. The final radiomic signature was used as input to a fully connected deep neural network (three hidden layers; ReLU activation; dropout 0.3) implemented in TensorFlow/Keras (version 2.10; Google LLC, Mountain View, CA, USA). The internal cohort was split 70:30 into training and validation subsets using stratified random sampling; the external cohort served as an independent test set with no overlap.[18,19]

Statistical Analysis

Statistical analyses were conducted utilizing SPSS version 22.0 (IBM Corp., Armonk, NY, USA) and GraphPad Prism version 8.0 (GraphPad Software, San Diego, CA, USA). Continuous variables are presented as means ± standard deviation and were compared employing independent samples t-tests; categorical variables are presented as frequencies and percentages and were analyzed using the chi-square test or Fisher's exact test, as appropriate. Receiver operating characteristic (ROC) curve analysis was performed to assess the diagnostic efficacy of the model and individual radiomic features. The area under the curve (AUC), sensitivity, specificity, accuracy, positive predictive value (PPV), and negative predictive value (NPV) were calculated. Optimal cutoff points were identified using the Youden index. A *p*-value of less than .05 was deemed statistically significant.

Ethical Statement

This retrospective study was approved by the Ethics Committee of the Mongolian National University of Medical Sciences. Due to the retrospective nature of the study, the requirement for written informed consent was waived.

Results

Patient Characteristics

Of 168 patients initially screened, 47 were excluded according to the predefined criteria, yielding a final internal cohort of 121 patients with histopathologically confirmed RCC or related neoplasm (Figure 1). The mean age was 55.3 ± 13.1 years, and 57 (47.1%) were male. Patients were stratified into ccRCC (n = 84) and non-ccRCC (n = 37) groups. Mean tumor volume was 88.4 ± 71.2 cm^3, and most tumors were exophytic in location (n = 89, 73.6%). Among ccRCC cases, Fuhrman grade II was the most common (46.4%). Within the non-ccRCC group, angiomyolipoma (35.1%), papillary RCC (18.9%), and chromophobe RCC (16.2%) were the most frequent diagnoses. Baseline characteristics stratified by subtype are summarized in Table 1. A statistically significant difference was observed between groups for sex distribution (p = .043), with male predominance in ccRCC; other baseline variables did not differ significantly between subtypes.

Table 1. Baseline patient characteristics stratified by RCC subtype (internal cohort, n = 121).

Characteristics	All (n=121)	ccRCC (n=84)	non-ccRCC (n=37)	*p*-value
Age (years), mean ± SD	55.3 ± 13.1	53.8 ± 11.6	58.4 ± 15.1	.134
Sex, n (%)				
Male	57 (47.1)	45 (53.6)	12 (32.4)	.043
Female	64 (52.9)	39 (46.4)	25 (67.6)	—
Tumor laterality, n (%)				
Right	59 (48.8)	40 (47.6)	19 (51.4)	.718
Left	62 (51.2)	44 (52.4)	18 (48.6)	—
Tumor location, n (%)				
Exophytic	89 (73.6)	63 (75.0)	26 (70.3)	.580
Endophytic	23 (19.0)	16 (19.0)	7 (18.9)	—
Mesophytic	9 (7.4)	5 (6.0)	4 (10.8)	—
Tumor volume (cm^3), mean ± SD	88.4 ± 71.2	96.3 ± 76.8	71.2 ± 55.4	.081
≤ 117 cm^3	91 (75.2)	62 (73.8)	29 (78.4)	.597
> 117 cm^3	30 (24.8)	22 (26.2)	8 (21.6)	—
Fuhrman grade (ccRCC only), n (%)				
Grade I	14 (16.7)	14 (16.7)	—	—
Grade II	39 (46.4)	39 (46.4)	—	—
Grade III	23 (27.4)	23 (27.4)	—	—
Grade IV	8 (9.5)	8 (9.5)	—	—
Histopathological subtype, n (%)				
Clear cell (ccRCC)	84 (69.4)	84 (100)	—	—
Angiomyolipoma (AML)	13 (10.7)	—	13 (35.1)	—
Papillary (pRCC)	7 (5.8)	—	7 (18.9)	—
Chromophobe (chRCC)	6 (5.0)	—	6 (16.2)	—
Oncocytoma	6 (5.0)	—	6 (16.2)	—
Oncocytic neoplasm	1 (0.8)	—	1 (2.7)	—
Other	4 (3.3)	—	4 (10.8)	—

SD = standard deviation; ccRCC = clear cell renal cell carcinoma; non-ccRCC = non–clear cell RCC. — = not applicable. Continuous variables compared using independent samples t test; categorical variables using chi-square or Fisher exact test. p < .05 considered statistically significant

Radiomic Feature Analysis

Following LASSO feature selection, GLRLM-derived metrics emerged as the strongest discriminators between ccRCC and non-ccRCC. The GLRLM feature differed significantly between groups (median 0.158 vs 0.119; p < .001), with an optimal cutoff of 0.1493 identified by the Youden index. First-order uniformity (cutoff 0.0892, $p < .001$) and variance (cutoff 41.7, $p < .001$) were the next most informative features. Figure 3 illustrates the distribution of GLRLM and first-order uniformity values and the AUC ranking of the top 10 discriminative features.

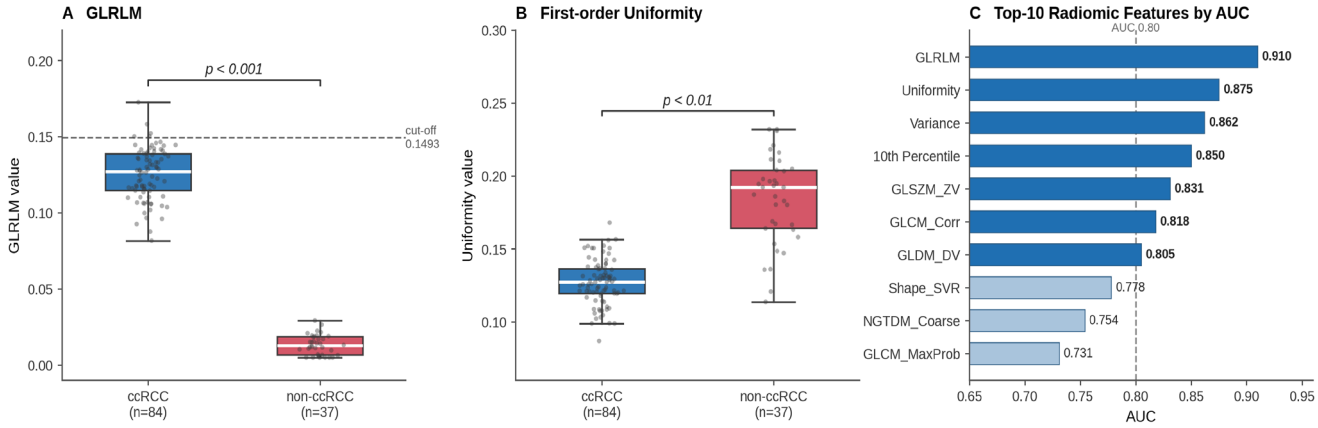

Figure 3. Radiomic feature analysis. (A) Box-strip plot of GLRLM values in ccRCC and non-ccRCC groups (p < .001); the dashed line indicates the optimal cutoff (0.1493). (B) Box-strip plot of first-order uniformity values ($p < .01$). (C) Horizontal bar chart showing AUC values for the top 10 discriminative radiomic features; darker bars indicate AUC ≥ 0.80.

Diagnostic Model Performance — Internal Validation

The radiomics–deep learning model achieved excellent diagnostic performance in the internal validation cohort, with AUC = 0.92 (95% CI, 0.86–0.96), sensitivity 83.3%, specificity 92.3%, and accuracy 86.0% at the optimal GLRLM cutoff (Youden index). Of 84 ccRCC cases, 70 (83.3%) were correctly classified; of 37 non-ccRCC cases, 34 (91.9%) were correctly classified (Figure 5A). ROC curves for the leading features are shown in Figure 4A.

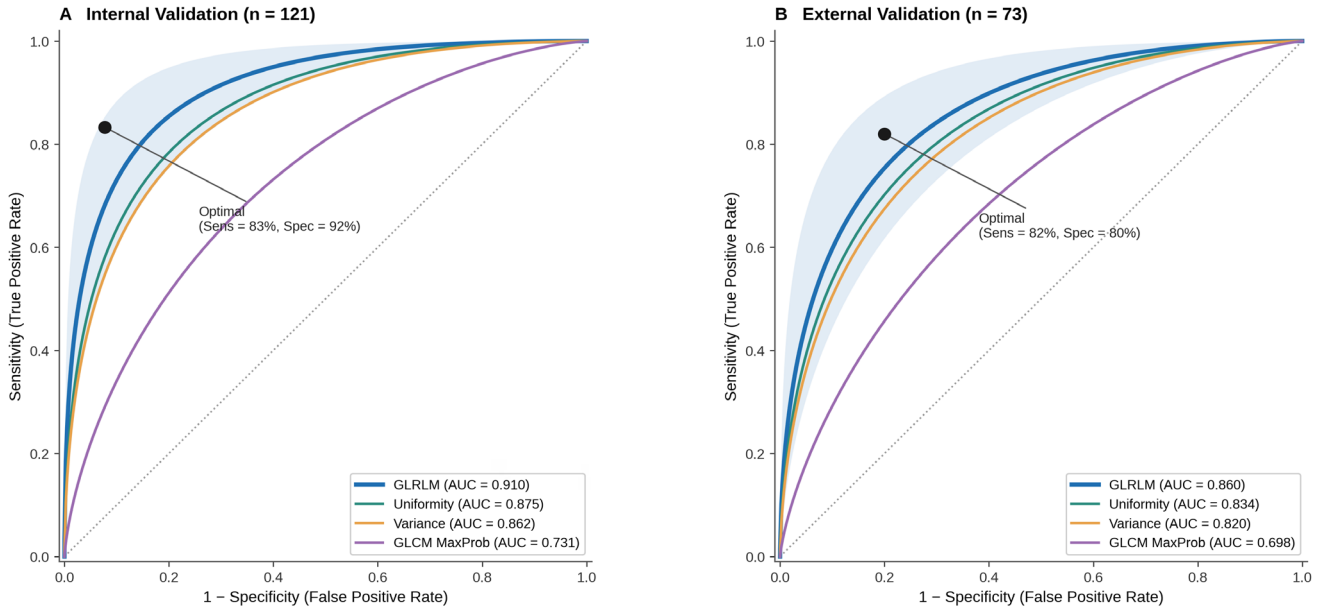

Figure 4. ROC curves for discrimination of ccRCC versus non-ccRCC. (A) Internal cohort (n = 121): GLRLM AUC = 0.910, sensitivity 83.3%, specificity 92.3% at the optimal cutoff. (B) External cohort (n = 73): GLRLM AUC = 0.860, sensitivity 82.0%, specificity 80.0%. Shaded areas represent 95% confidence intervals; different line weights distinguish features.

External Validation

In the independent external cohort (n = 73; 50 ccRCC, 23 non-ccRCC), the model maintained robust diagnostic performance with AUC = 0.86 (95% CI, 0.79–0.93), sensitivity 82.0%, specificity 80.0%, and accuracy 80.8%. Of 50 ccRCC cases, 41 (82.0%) were correctly classified; of 23 non-ccRCC cases, 18 (78.3%) were correctly classified (Figure 5B). The modest decrement in performance compared with the internal cohort (AUC 0.92 – 0.86) is consistent with expected inter-institutional variability in imaging protocols and indicates that the model captures transferable rather than dataset-specific features.

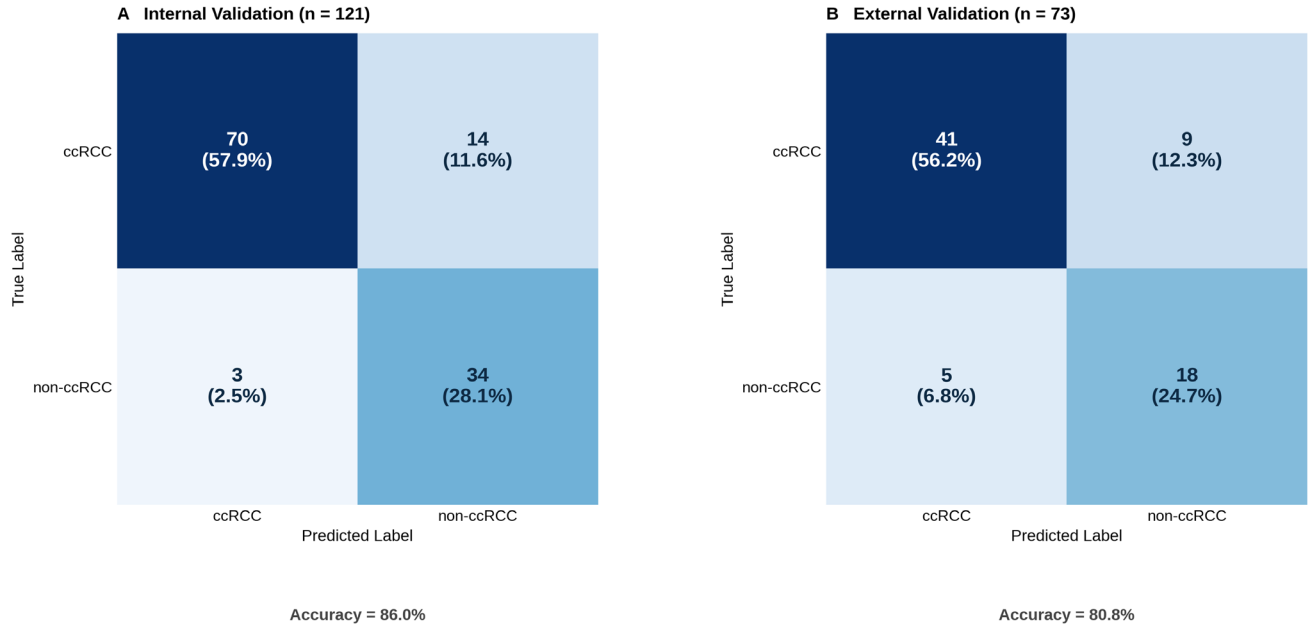

Figure 5. Confusion matrices for the radiomics–deep learning classification model. (A) Internal cohort (n = 121): overall accuracy 86.0%; ccRCC correctly classified in 70/84 (83.3%), non-ccRCC in 34/37 (91.9%). (B) External cohort (n = 73): overall accuracy 80.8%; ccRCC 41/50 (82.0%), non-ccRCC 18/23 (78.3%).

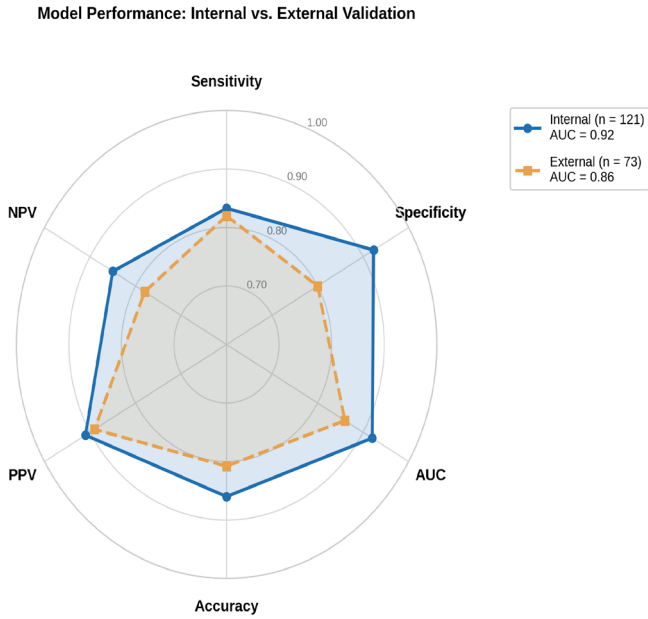

Figure 6. Radar (spider) chart comparing six diagnostic performance metrics between internal (n = 121, solid line) and external (n = 73, dashed line) validation cohorts: AUC, sensitivity, specificity, accuracy, PPV, and NPV. Internal: AUC = 0.92, sensitivity = 83.3%, specificity = 92.3%, accuracy = 86.0%, PPV = 91%, NPV = 85%. External: AUC = 0.86, sensitivity = 82.0%, specificity = 80.0%, accuracy = 80.8%, PPV = 89%, NPV = 78%.

Summary of Diagnostic Performance

Overall, the radiomics–deep learning model demonstrated high discriminative ability for RCC subtype classification, with consistent performance across internal and external datasets and a major contribution from GLRLM features.

Table 2. Diagnostic performance of the leading radiomic features for ccRCC versus non-ccRCC differentiation in the internal and external validation cohorts.

Feature	AUC	Sensitivity (%)	Specificity (%)	Accuracy (%)	95% CI (AUC)	*p*-value
Internal validation cohort (n=121)						
GLRLM	0.910	83.3	92.3	86.0	0.857–0.964	< .001
First-order Uniformity	0.875	81.0	89.5	84.2	0.821–0.938	< .001
Variance	0.862	79.8	87.2	83.5	0.799–0.925	< .001
10th Percentile	0.850	78.5	85.3	82.0	0.780–0.920	< .001
GLSZM Zone Variance	0.831	76.2	84.0	80.1	0.756–0.906	< .001
GLCM Correlation	0.818	74.5	82.0	78.5	0.742–0.894	< .001
GLDM Dependence Variance	0.805	73.1	80.5	77.2	0.729–0.881	< .001
Shape SVR	0.778	70.8	78.3	74.5	0.694–0.862	< .001
NGTDM Coarseness	0.754	68.4	76.0	72.1	0.668–0.840	.002
GLCM MaxProbability	0.731	67.2	74.6	71.0	0.637–0.825	.002
Flatness	0.584	57.1	61.4	58.7	0.490–0.678	.142
External validation cohort (n = 73)						
GLRLM	0.860	82.0	80.0	80.8	0.789–0.931	< .001
First-order Uniformity	0.834	79.2	78.5	83.1	0.751–0.917	< .001
Variance	0.820	77.8	76.9	82.0	0.737–0.903	< .001

AUC = area under the ROC curve; CI = confidence interval. Sensitivity and specificity were calculated at the optimal cutoff (Youden index). GLRLM = gray-level run-length matrix; GLCM = gray-level co-occurrence matrix; GLSZM = gray-level size zone matrix; GLDM = gray-level dependence matrix; NGTDM = neighborhood gray-tone difference matrix; SVR = surface-to-volume ratio. Flatness did not reach statistical significance (p = .142).

Discussion

In this study, we demonstrated that CT-based radiomics combined with a deep learning approach can accurately differentiate RCC subtypes preoperatively. The model achieved excellent diagnostic performance in the internal cohort (AUC = 0.92) and maintained robust performance in the external validation cohort (AUC = 0.86), supporting its potential clinical applicability. These findings suggest that radiomics-derived quantitative features capture tumor characteristics that are not readily appreciable through conventional visual assessment.[21,22,32]

The observed performance can be explained by the radiomic features' ability to quantify intratumoral heterogeneity. RCC exhibits substantial variability in cellular architecture, vascularity, and necrosis, all of which are closely related to histopathological subtype. Among the evaluated features, GLRLM parameters demonstrated the strongest discriminative power. GLRLM features quantify the distribution and length of homogeneous gray-level runs, thereby reflecting tumor texture and structural organization. In ccRCC, typically characterized by heterogeneous enhancement patterns and increased vascularity, these features differ significantly from those of non-ccRCC subtypes, supporting their biological relevance. [21,22]

Our findings are consistent with previous radiomics studies reporting high diagnostic performance for RCC subtype differentiation using CT-based texture analysis. Varghese, et al.[23] reported that radiomic features could differentiate benign and malignant renal masses with AUC values ranging from 0.80 to 0.98. Similarly, Wentland, et al.[24] demonstrated that machine learning models based on CT radiomics achieved a diagnostic accuracy of approximately 82%. Feng, et al.[25] further showed that radiomics-based models could effectively differentiate renal

tumor subtypes, highlighting the added value of quantitative imaging features compared with conventional clinical parameters. Hoang, et al.[33] also reported high sensitivity for subtype differentiation using multiphasic imaging–based texture analysis. Together, these findings support the reproducibility and reliability of radiomics in RCC characterization.

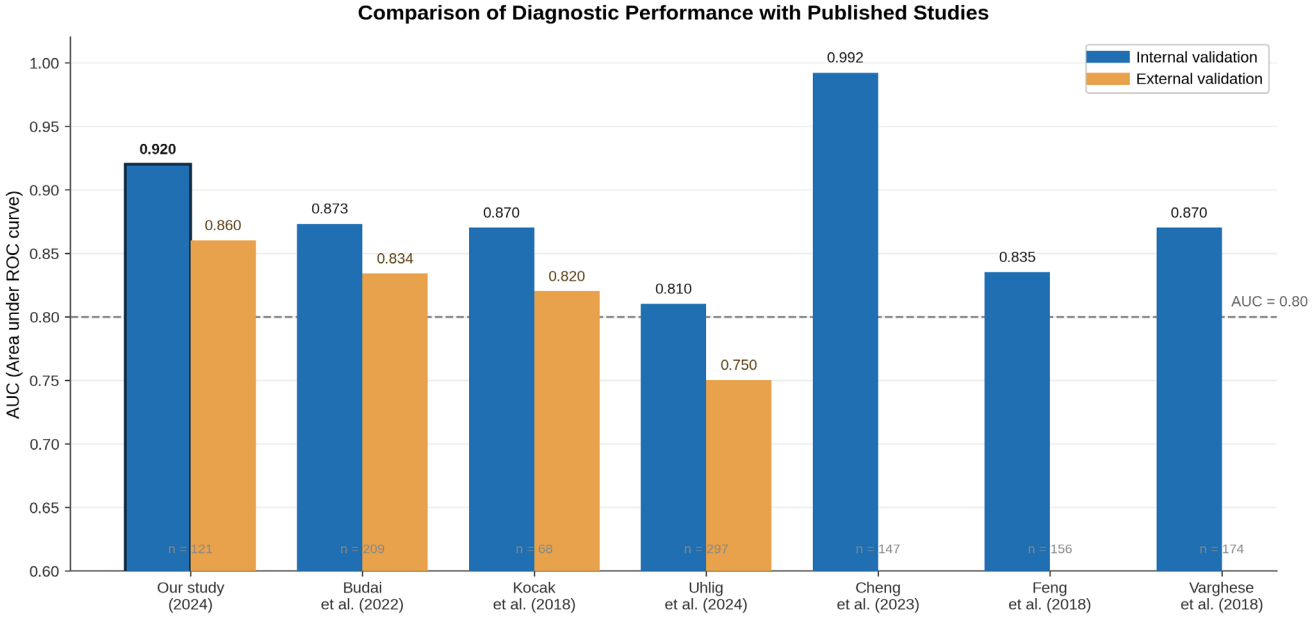

Figure 7. **Comparison of diagnostic performance (AUC) of the present radiomics model with published CT-based RCC subtype-differentiation studies. Darker bars represent internal validation AUC; lighter bars represent external validation AUC where available. Our study (leftmost group) achieved the highest internally validated AUC (0.920) with robust external generalizability (AUC = 0.860). The dashed line indicates AUC = 0.80. Sample sizes (n) are shown at the base of each bar group.**

The inclusion of external validation represents a key strength of this study. Many prior studies have been limited to single-center datasets, which restricts their generalizability. Kocak, et al.[31] incorporated external validation and demonstrated stable performance across independent datasets. In our study, although a moderate decrease in performance was observed in the external cohort, this is expected due to inter-institutional variability in imaging protocols, scanner characteristics, and patient populations. Radiomic features are inherently sensitive to such variations, leading to domain shift between datasets. Importantly, the relatively small performance drop (AUC from 0.92 to 0.86) indicates that the model captures robust, transferable imaging features rather than dataset-specific patterns, supporting its generalizability.[7,31]

Inter-observer reproducibility is a recognized concern in radiomic studies. In our analysis, two radiologists independently performed all segmentations, and feature stability was quantified using the ICC. The retained feature set yielded excellent agreement (ICC = 0.91; 95% CI, 0.87–0.94), indicating that the model's performance is not unduly influenced by segmentation variability. Future implementation of deep learning–based automated segmentation may further reduce observer dependence.

Despite these promising results, several limitations should be acknowledged. First, the relatively small sample size may limit statistical power and generalizability. Second, the retrospective single-center design introduces potential selection bias. Third, although inter-observer reproducibility was excellent, tumor segmentation was performed manually, and fully automated pipelines may improve scalability. Fourth, the study did not incorporate genomic or molecular data; previous studies have suggested that combining radiomics with genomic information (radiogenomics) may further improve predictive performance and provide deeper biological insight.[22,32]

Future research should concentrate on large-scale, multi-center prospective validation to strengthen the robustness and clinical relevance of radiomics-based models. The adoption of automated segmentation employing deep learning techniques could enhance reproducibility, while integrating radiomics with genomic, proteomic, and clinical data may facilitate the development of more comprehensive predictive frameworks, thereby advancing the field of precision oncology. Furthermore, standardization of imaging protocols alongside the

implementation of harmonization techniques will be critical in reducing variability and ensuring reproducibility across different institutions.[31,33,34]

Conclusion

CT-based radiomics represents a promising non-invasive approach for preoperative RCC subtype prediction. By capturing tumor heterogeneity and providing quantitative imaging biomarkers, radiomics has the potential to support clinical decision-making and facilitate personalized treatment strategies.

Conflict of Interest

The authors declare no conflict of interest, financial or otherwise.

Funding

This research was supported by a grant from the National Foundation for Science and Technology, Mongolia.

Acknowledgments

The authors thank the medical and technical staff of the Diagnostic Imaging Center and the Urology-Andrology Center of The First Central Hospital of Mongolia for their support in data collection and patient care.

Authors Contribution

Enkhbold Sereejav: ORCID https://orcid.org/0009-0008-7892-6758, Conceptualization, formal analysis, methodology, resources, writing original draft, writing review and editing.

Purevdorj Otgonbayar: ORCID https://orcid.org/0009-0000-2137-5424, Data curation.

Telmen Khuvituguldur: ORCID https://orcid.org/0009-0008-2385-0549, Data curation, writing original draft.

Sodgerel Bold: ORCID https://orcid.org/0009-0006-6470-3882, Formal analysis, data curation.

Shiirevnyamba Avirmed: ORCID https://orcid.org/0000-0002-1010-8221, Resources, supervision, writing review and editing.

Gonchigsuren Dagvasumberel: ORCID https://orcid.org/0000-0002-8265-6024, Methodology, writing review and editing.

Oyunbold Lamid-Ochir: ORCID https://orcid.org/0000-0002-0709-3794, Investigation, conceptualization, supervision, writing review and editing.

Reference

1. Sheth S, Scatarige JC, Horton KM, et al. Current concepts in the diagnosis and management of renal cell carcinoma: role of multidetector CT and three-dimensional CT. *Radiographics*. 2001;21:S237-S254. https://doi.org/10.1148/radiographics.21.suppl_1.g01oc18s237
2. Catalano C, Fraioli F, Laghi A, et al. High-resolution multidetector CT in the preoperative evaluation of patients with renal cell carcinoma. *AJR Am J Roentgenol*. 2003;180(5):1271-1277. https://doi.org/10.2214/ajr.180.5.1801271
3. Johnson CD, Dunnick NR, Cohan RH, et al. Renal adenocarcinoma: CT staging of 100 tumors. *AJR Am J Roentgenol*. 1987;148(1):59-63. https://doi.org/10.2214/ajr.148.1.59
4. Fein AB, Lee JK, Balfe DM, et al. Diagnosis and staging of renal cell carcinoma: a comparison of MR imaging and CT. *AJR Am J Roentgenol*. 1987;148(4):749-753. https://doi.org/10.2214/ajr.148.4.749
5. Sun M, Zhou Y, Zhao Z, et al. CT-based radiomics for prediction of distant metastasis in clear cell renal cell carcinoma. *Eur Radiol*. 2022;32(4):2305-2314. https://doi.org/10.1007/s00330-021-08376-w
6. Shan S, Zhang Y, Li J, et al. A clinicoradiomics model for progression-free survival in renal cell carcinoma. *Eur J Radiol*. 2025;180:111234. https://doi.org/10.1016/j.ejrad.2024.111234
7. Liu H, Chen Y, Zhang X, et al. Multiphase CT-based radiomics model for risk stratification in renal cell carcinoma. *Insights Imaging*. 2023;14(1):26. https://doi.org/10.1186/s13244-023-01378-w
8. Zannotti A, Carconi C, Carozza R, et al. The role of radiomics in renal mass characterization. *J Med Imaging Radiat Oncol*. 2024;68(2):210-218. https://doi.org/10.1111/1754-9485.13616
9. Zheng Z, Chen Z, Xie Y, et al. Development and validation of a CT-based nomogram for preoperative prediction of clear cell

renal cell carcinoma grades. *Eur Radiol*. 2021;31(8):6078-6086. https://doi.org/10.1007/s00330-020-07667-y

10. Wang R, Yang L, Huang J, et al. A radiomics nomogram for preoperative prediction of WHO/ISUP grade in clear cell renal cell carcinoma. *Front Oncol*. 2021;11:543854. https://doi.org/10.3389/fonc.2021.543854
11. Wang P, Li H, Liu X, et al. A radiomics-based nomogram for preoperative grading of renal cell carcinoma. *Sci Rep*. 2021;11(1):15001. https://doi.org/10.1038/s41598-021-94319-w
12. Nazari M, Shiri I, Hajianfar G, et al. Radiomics-based machine learning model for Fuhrman grade prediction in clear cell renal cell carcinoma. *Comput Biol Med*. 2019;108:10-18. https://doi.org/10.1016/j.compbiomed.2019.03.011
13. Nie P, Yang G, Wang Y, et al. A CT-based deep learning radiomics nomogram outperforms the existing prognostic models for outcome prediction in clear cell renal cell carcinoma: a multicenter study. *Eur Radiol*. 2023;33(12):8858-8868. https://doi.org/10.1007/s00330-023-09869-6
14. Birnbaum BA, Jacobs JE, Ramchandani P. Multiphasic renal CT: comparison of renal mass enhancement during the corticomedullary and nephrographic phases. *Radiology*. 1996;200(3):753-758. https://doi.org/10.1148/radiology.200.3.8756927
15. Yuh BI, Cohan RH. Different phases of renal enhancement: role in detecting and characterizing renal masses during helical CT. *AJR Am J Roentgenol*. 1999;173(3):747-755. https://doi.org/10.2214/ajr.173.3.10470916
16. Young JR, Margolis D, Sauk S, et al. Clear cell renal cell carcinoma: discrimination from other renal cell carcinoma subtypes and oncocytoma at multiphasic multidetector CT. *Radiology*. 2013;267(2):444-453. https://doi.org/10.1148/radiol.13112617
17. Lee-Felker SA, Felker ER, Tan N, et al. Qualitative and quantitative MDCT features for differentiating clear cell renal cell carcinoma from other solid renal cortical masses. *AJR Am J Roentgenol*. 2014;203(5):W516-W524. https://doi.org/10.2214/AJR.14.12460
18. Coy H, Young JR, Douek ML, et al. Quantitative computer-aided diagnostic algorithm for automated detection of peak lesion attenuation in differentiating clear cell from papillary and chromophobe renal cell carcinoma, oncocytoma, and fat-poor angiomyolipoma on multiphasic multidetector computed tomography. *Abdom Radiol (NY)*. 2017;42(7):1919-1928. https://doi.org/10.1007/s00261-017-1095-6
19. Kim SH, Kim CS, Kim MJ, et al. Differentiation of clear cell renal cell carcinoma from other subtypes and fat-poor angiomyolipoma by use of quantitative enhancement measurement during three-phase MDCT. *AJR Am J Roentgenol*. 2016;206(1):W21-W28. https://doi.org/10.2214/AJR.15.14666
20. Ruppert-Kohlmayr AJ, Uggowitzer M, Meissnitzer T, et al. Differentiation of renal clear cell carcinoma and renal papillary carcinoma using quantitative CT enhancement parameters. *AJR Am J Roentgenol*. 2004;183(5):1387-1391. https://doi.org/10.2214/ajr.183.5.1831387
21. Lin P, Lin YQ, Gao RZ, et al. Radiomic profiling of clear cell renal cell carcinoma reveals subtypes with distinct prognosis and molecular pathways. *Transl Oncol*. 2021;14(1):100959. https://doi.org/10.1016/j.tranon.2020.100959
22. Alessandrino F, Shinagare AB, Bosse D, et al. Radiogenomics in renal cell carcinoma. *Abdom Radiol (NY)*. 2019;44(6):1990-1998. https://doi.org/10.1007/s00261-018-1624-y
23. Varghese BA, Chen F, Hwang DH, et al. Differentiation of predominantly solid enhancing lipid-poor renal cell masses by use of contrast-enhanced CT: evaluating the role of texture in tumor subtyping. *AJR Am J Roentgenol*. 2018;211(6):W288-W296. https://doi.org/10.2214/AJR.18.19551
24. Wentland AL, Yamashita R, Kino A, et al. Differentiation of benign from malignant solid renal lesions using CT-based radiomics and machine learning: comparison with radiologist interpretation. *Abdom Radiol (NY)*. 2023;48(2):642-648. https://doi.org/10.1007/s00261-022-03735-7
25. Feng Z, Rong P, Cao P, et al. Machine learning–based quantitative texture analysis of CT images of small renal masses: differentiation of angiomyolipoma without visible fat from renal cell carcinoma. *Eur Radiol*. 2018;28(4):1625-1633. https://doi.org/10.1007/s00330-017-5118-z
26. Zhang H, Yin F, Chen M, et al. A CT-based radiomics model for differentiating renal cell carcinoma subtypes. *Front Oncol*. 2021;11:617010. https://doi.org/10.3389/fonc.2021.617010
27. Yao N, Hu H, Chen K, et al. Deep learning for renal cell carcinoma subtype classification using CT imaging. *Med*

Image Anal. 2023;85:102750. https://doi.org/10.1016/j.media.2023.102750

28. Aymerich M, Ortega R, García-Baizán A, et al. Radiomics-based classification of clear cell renal cell carcinoma. *Diagnostics (Basel)*. 2025;15(11):1337. https://doi.org/10.3390/diagnostics15111337
29. Han S, Hwang SI, Lee HJ. The classification of renal cancer in 3-phase CT images using a deep learning method. *J Digit Imaging*. 2019;32(4):638-643. https://doi.org/10.1007/s10278-019-00230-2
30. Uhlig A, Uhlig J, Leha A, et al. Radiomics and machine learning for renal tumor subtype assessment using multiphase computed tomography in a multicenter setting. *Eur Radiol*. 2024;34(9):6254-6263. https://doi.org/10.1007/s00330-024-10731-6
31. Kocak B, Yardimci AH, Bektas CT, et al. Textural differences between renal cell carcinoma subtypes: machine learning–based quantitative computed tomography texture analysis with independent external validation. *Eur J Radiol*. 2018;107:149-157. https://doi.org/10.1016/j.ejrad.2018.08.014
32. Karlo CA, Di Paolo PL, Chaim J, et al. Radiogenomics of clear cell renal cell carcinoma: associations between CT imaging features and mutations. *Radiology*. 2014;270(2):464-471. https://doi.org/10.1148/radiol.13130663
33. Hoang UN, Mojdeh Mirmomen S, Meirelles O, et al. Assessment of multiphasic contrast-enhanced MR imaging–based radiomic features for differentiating renal cell carcinoma subtypes. *Sci Rep*. 2018;8(1):1238. https://doi.org/10.1038/s41598-018-19503-x
34. Wu Y, Cao F, Lei H, et al. Interpretable multiphasic CT-based radiomic analysis for preoperatively differentiating benign and malignant solid renal tumors: a multicenter study. *Abdom Radiol (NY)*. 2024;49(9):3096-3106. https://doi.org/10.1007/s00261-024-04351-3